SIMULATING BEHAVIOUR OF UNREINFORCED AND REINFORCED MASONRY WALL PANELS UNDER MONOTONIC LATERAL LOADING

Anil Kasula [1] [*]**, Manjip Shakya**[2]**, Sudip Karajnit**[3]**, Amit Prajapati**[4]

[1] Department of Civil Engineering, Khwopa College of Engineering, Tribhuvan University, Nepal
[2] PG Department of Earthquake Engineering, Khwopa Engineering College,
Purbanchal University, Nepal
[3] Department of Civil Engineering, Khwopa Engineering College, Purbanchal University, Nepal
[4] State Key Laboratory of Disaster Reduction in Civil Engineering, Tongji University, China

Abstract

Unreinforced Masonry (URM) structures are extremely vulnerable to seismic activities. Under seismic loads, the failure of these structures is either due to in-plane failure or an out-of-plane failure mechanism. Different seismic retrofitting and strengthening strategies for masonry structures have been developed and implemented in recent decades. The performance of existing URM structures can be greatly improved by retrofitting. This paper uses steel strips with anchor bolt arrangement as reinforcing material for retrofitting purposes. A comparative study of change in lateral load carrying capacity of unreinforced and reinforced masonry wall panels under in-plane lateral load based on numerical simulation is presented in this study. Initially, a 3D numerical model of the URM wall panel is prepared in ABAQUS FEM using Simplified Micro Modelling (SMM) technique. The Concrete Damage Plasticity (CDP) model is used as a material model and the surface-based coupled cohesion-friction model as the interface material. The response of the URM wall panel under displacement-controlled monotonic lateral load is evaluated and validated against experimental results. Another separate numerical model of reinforced masonry is prepared with identical mechanical properties. A comprehensive study is conducted on the change in the performance of both wall panels. The study found that the ultimate load-carrying capacity of reinforced masonry wall panels is increased by 22% compared to the unreinforced masonry wall panel.

1. Introduction

Masonry is one of the most commonly used non-homogenous construction materials, which has been used for thousands of years. Although masonry is an ancient and out dated construction material, it is widely used and favored in some countries. The most prevalent kind of URM is Masonry Heritage Structures, which offer value settings such as aesthetic, social, archaeological, cultural, economic, and technological, making them a true treasury of human civilization. The preservation and conservation of such historic URM structures is a serious problem for structure engineers today. The design, building methods, and original materials employed in such historic masonry structures make them extremely vulnerable in the present. Similarly, for new construction, it has always been difficult to identify and characterize the structural performance of masonry due to its heterogeneous complicated characteristics and strong nonlinear response of components which make it a vulnerable structure. As a result, it is frequently necessary for URM structures to be reinforced during new construction while existing plane masonry must be retrofitted to lessen the likelihood of failure. When subjected to seismic loads, the URM structures mostly undergo in-plane and out-of-plane failure. Sometimes, brittle failure of masonry components due to imposed horizontal racking loads apart

---
[*]Corresponding author: Anil Kasula
Department of Civil Engineering, Khwopa College of Engineering
Email: kasula3650@gmail.com

from existing gravity loads, take place leading to the possible collapse of structures. Due to these reasons, the URM structures may be required to be strengthened or retrofitted to ensure effective performance under seismic tremors. Different technical approaches have been developed and implemented to strengthen the seismic performance of URM structures. Many strengthening or retrofitting methods, however, have only been investigated for individual cases, making it impossible to extrapolate the findings to situations involving other construction materials or systems. The analytical techniques are not reliable enough to determine the seismic performance of retrofitted masonry structures as the retrofitting method may work differently in masonry structures made of different materials. The majority of earlier research was experimental only. In the experimental approach, the long-term behavior between masonry-strengthening interfaces is not known clearly , which makes it unpopular. However, numerical simulation can be a powerful tool in such studies and can be used to analyze the seismic performance of retrofitted masonry regarding the efficiency of retrofitting. Although many retrofitting and strengthening tests have been conducted over the past few decades, only a small portion of them have been numerically modeled Wang et al., 2018. There seems to be a lack of research work exploring the change in ultimate shear strength of masonry walls reinforced using steel battens on the surface under monotonic in-plane loading conditions. In this paper, analytical modeling of an unreinforced and reinforced masonry wall with the same mechanical characteristics is carried out separately using the SMM approach in ABAQUS software to study the changes in ultimate shear strength. Steel battens and anchor rods are used on both sides of walls for reinforcing purposes.

2. Finite Element Modeling

The 3D model of a masonry wall is prepared using an SSM approach. The masonry units are modeled as a continuum element by expanding up to half of the mortar thickness in the horizontal and vertical direction to overcome wall size while the mortar joints are modeled as zero thickness interface discontinuous element in ABAQUS. The proposed model simulates the 3D behavior of masonry assemblage representing the crushing of masonry units under compression and initiation of cracks and its propagation along masonry joints without defining an initial crack location. The simulation is performed under a quasi-static monotonic in-plane loading process using an ABAQUS/explicit solver. The explicit dynamic solver employs a central difference integration scheme that operates without iteration, which is an essential trait of the implicit solver. Unlike considering iteration to secure desired convergence tolerance in implicit procedures, ABAQUS/ explicit performs analysis without considering equilibrium conditions using a large number of small-time increments. The progression of analysis in the time domain is performed by using many small increments guided by a numerical stability criterion Aref and Dolatshahi, 2013.

2.1. Modelling of Masonry Units

The expanded masonry units are modeled using solid 3D continuum elements C3D8R with reduced integration. The reduced integration for the element is based on a single point uniform strain formulation where the strains are obtained as average strain over the element volume. The element with reduced integration possesses a problem of hour-glassing or zero energy deformation mode. Hour-glassing is a condition when there is deformation in the element but there is no strain and is prevented by adopting an enhanced hour-glassing control scheme in ABAQUS/explicit. The expanded masonry units are modified to have an equivalent elastic response to the original masonry assemblage, as Kurdo et al., 2017 suggested. The CDP model, generally used to simulate the nonlinear behavior of reinforced or plain concrete and other brittle materials is used to represent the material non-linearity of masonry units. The CDP model can simulate the initiation and progression of material damage, such as cracking and crushing, shear failure, and post-peak softening with different material properties in both tension and compression which are crucial for accurately capturing the behavior of masonry structures. Our study relies on two principal failure modes, cracking in tension and crushing in compression. It uses concepts of isotropic damaged elasticity in combination with isotropic tensile and non-associated multi-hardening compressive plasticity to represent the inelastic behavior and irreversible damage of elements that occur during the fracturing process. The stiffness degradation in the softening zone for both tension and compression is represented by the damage variable and is based on the energy equivalence principle as suggested by Lubliner et al., 1989. For yield surface in the CDP model, the yield functions based upon failure criteria initially proposed by Lubliner et al., 1989 and modified by Lee and Fenves, 1998 are used to describe plasticity under tension and compression in FE models. Different CDP parameters defined as dilation angle (ψ), flow potential eccentricity (ϵ), ratio of biaxial/uniaxial compressive strength (σ_{bo}/σ_{co}), ratio of second stress invariant (K_c), weight factor in tension (w_t) and weight factor in compression (w_c) used in ABAQUS for proposed 3D finite element simplified micro model is shown in Table 1.

Table 1: CDP parameters with default value in ABAQUS to determine yield surface (Qingfu et al., 2020)

Parameter	ψ	ϵ	σ_{bo}/σ_{co}	K_c	w_t	w_c
Values	30	0.1	1.16	0.67	0	1

The compressive and tensile stress-strain relationship for the masonry block and mortar joint is obtained from relations as suggested by Zhang et al., 2017) represented by Equation 1 and Equation 2.

$$\sigma_{cu} = \frac{h}{1 + (h-1)x_c^{h/(h-1)}} E_u \varepsilon_c \qquad (1)$$

The compressive stress (σ_{cu}) of masonry units depends upon corresponding compressive strain (ε_c), the ratio of compressive strain to peak compression strain given by $x_c = \varepsilon_c/\varepsilon_{cu}$, the elastic modulus of masonry unit (E_u) and compressive factor (h) whose value is 1.633.

$$\sigma_{tu} = \begin{cases} x_t E_u \varepsilon_t, & x_t \leq 1 \\ \frac{x_t}{2(x_t-1)^{1.7} + x_t} E_u \varepsilon_t, & x_t > 1 \end{cases} \qquad (2)$$

Likewise, the tensile stress (σ_{tu}) of masonry unit is dependent on elastic modulus (E_u), compressive factor (h) taken as 1.633, corresponding tensile strain (ε_t) and the ratio of tensile strain to peak tensile strain given by $x_t = \varepsilon_t/\varepsilon_{tu}$.

Under the action of compressive and tensile stresses, the masonry units undergo stiffness degradation known as the damage variable. The damage variable (d) for compression or tension depends on compressive or tensile stress (σ), corresponding compressive or tensile strain (ε), and initial elastic modulus (E_o) represented by Equation 3.

$$d = 1 - \sqrt{\frac{\sigma}{E_o \varepsilon}} \qquad (3)$$

The value of the damage variable ranges between 0 and 1 considering the damage occurs only in softening.

The elastic response of the joint interface for linear elastic stage is represented by the equivalent stiffness proposed by Lourenço, 1996. The normal stiffness is dependent on the modulus of elasticity of both masonry units (E_u) and mortar (E_m) and the thickness of mortar (h_m) as given by Equation 4.

$$K_{nn} = \frac{E_u E_m}{h_m(E_u - E_m)} \qquad (4)$$

Likewise, the shear stiffness is dependent on the modulus of rigidity of masonry units (G_u) and mortar (G_m) and the thickness of mortar as given by Equation 5.

$$K_{ss} \ \& \ K_{tt} = \frac{G_u G_m}{h_m(G_u - G_m)} \qquad (5)$$

The nominal tensile traction vector (σ) in relation with the elastic stiffness matrix (K) and separation vector (Δ) is given by Equation 6.

$$\sigma = \begin{Bmatrix} \sigma_n \\ \tau_s \\ \tau_t \end{Bmatrix} = \begin{bmatrix} K_{nn} & 0 & 0 \\ 0 & K_{ss} & 0 \\ 0 & 0 & K_{tt} \end{bmatrix} \begin{Bmatrix} \Delta_n \\ \Delta_s \\ \Delta_t \end{Bmatrix} = K\Delta \qquad (6)$$

The plastic response of the joint interface is represented by damage initiation and damage evolution based on tractions between the interface which is dependent on fracture energy and frictional coefficient. For mixed mode failure mode, quadratic stress criteria is used to represent the initiation of degradation of a cohesive layer at the damage initiation point. The quadratic stress criteria are dependent on the tensile strength of mortar (σ_n^{max}), shear strength of mortar (τ_s^{max} & τ_t^{max}) in s and t direction and is represented by Equation 7. The Macaulay bracket in Equation 7 indicates the exclusion of compressive stress on fracture behavior of interface in the normal direction and shear strength of mortar is calculated using Mohr-Coulomb failure criteria.

$$\left(\frac{\langle \sigma_n \rangle}{\sigma_n^{\max}}\right)^2 + \left(\frac{\tau_s}{\tau_s^{\max}}\right)^2 + \left(\frac{\tau_t}{\tau_t^{\max}}\right)^2 = 1 \qquad (7)$$

After damage initiation, the loss of strength and failure of joints take place due to degradation of stiffness of the interface resulting from the propagation of cracks under damage evolution law represented by fracture energy with linear softening. The damage evolution law as addressed by Benzeggagh and Kenane, 1996 and represented by Equation 8 is dependent on critical fracture energy rate for mixed (G_{mf}), pure normal (G_{nf}), pure shear (G_{sf}) mode and a dimensionless parameter (m) take as 2 for quasi-brittle material (Kurdo et al., 2017).

$$G_{mf} = G_{nf} + (G_{sf} - G_{nf})\left(\frac{G_{sf}}{G_{nf} + G_{sf}}\right)^m \qquad (8)$$

The tensile and shear fracture energy rate is calculated based on the study by Lotfi and Shing, 1994 and Yuen et al., 2019 represented by Equation 9 to Equation 11.

$$G_{f,\min} = \frac{\sigma_n^2}{2K_{nn}} \qquad (9)$$

$$\text{G}_{\text{nf}} = 5\text{G}_{\text{f min}} \qquad (10)$$

$$\text{G}_{\text{sf}} = 10\text{G}_{\text{nf}} \qquad (11)$$

2.2. Modelling of interface material

Contact elements are used to simulate the interfaces between masonry units using an interface cohesive model combining damage (or de-bonding) and friction. The cohesion model is coupled together with the friction model in order to have continuous transition from development of cracks followed by propagation along masonry joints to pure frictional stage after de-cohesion.

2.2.1 Surface-based cohesion behavior

The cohesive interaction is a function of displacement separation between edges of potential cracks. Surface-based

cohesive behavior based on traction separation constitutive model along the bed and head joints is used to model linear and fracture behavior of zero thickness cohesive or bonded joints. The traction separation law is governed by three stages namely; linear-elastic traction separation stage, damage-initiation stage, and damage-evolution stage which allow mixed mode fracture and damage of cohesive surface in ABAQUS. Before the damage, this model assumes linear elastic behavior at the joint interface followed by propagation of damage represented by mixed tensile-shear fracture until the final fracture occurs under continuous loading.

2.2.2 Surface-based friction behavior

After the complete depletion of the cohesive surface between masonry units, the response of the interface joint is simulated using surface-based friction behavior based on normal and tangential behavior. The normal behavior allows adjacent masonry units to remain intact under compressive load until normal stress at the interface becomes zero and the formation of separation and cracking of units are initiated due to failure in tension. Hard contact behavior between adjacent masonry units is used which prevents penetration of masonry units over each other for normal behavior. The tangential behavior represents shear behavior between masonry units defined by a suitable frictional coefficient whose yielding criteria are based on the Coulomb friction model. Infinite elastic slip stiffness is adopted for this model. The slipping between adjacent surfaces is a function of shear stress. However, shear stress causing finite sliding is not considered. When the equivalent stress exceeds the critical friction stress defined by the friction model, the adjacent surfaces slide infinitely maintaining constant stress depending on the normal stress value.

2.3. Modelling of reinforcing materials

A Classical metal plasticity model with isotropic hardening behavior using standard Mises's yield surface is selected to represent the stress-strain relationship for steel anchor and steel battens used for reinforcing purposes considering linearly elastic-linearly plastic and identical in both tension and compression. The elastic modulus in the hardening zone is taken 1% of the initial elastic modulus. However, the steel beam used at the top of the masonry wall is modeled as a linearly elastic material

3. Model validation

3.1. Description of subject model

The experiment originally tested by Raijmakers and Vermeltfoort, 1992 and described by Lourenço, 1996 in his doctoral research is used for numerical simulation under monotonic loading using ABAQUS explicit solver. The
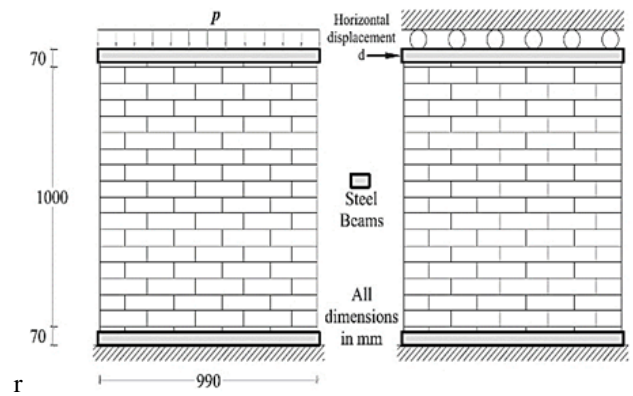

Figure 1: Experimental setup for TU Eindhoven shear wall

numerical model is TU Eindhovenn unreinforced masonry pier of 100 mm thickness with a width/height ratio of about unity (990mm x 1106mm), consisting of a total of 18 courses of solid clay bricks (full brick dimension 210 x 52 x 100 mm and half brick dimension 115 x 52 x 100 mm) and 10 mm thick mortar (1:2:9, cement : lime : sand by volume) as shown in Figure 1. In the simulation, the vertical movement of the top beam is restrained after applying imposed vertical compressive stress of 0.3 MPa and increasing monotonic load is horizontally applied to the wall via top beam under displacement control in a confined way.

3.2. Preparation of numerical model

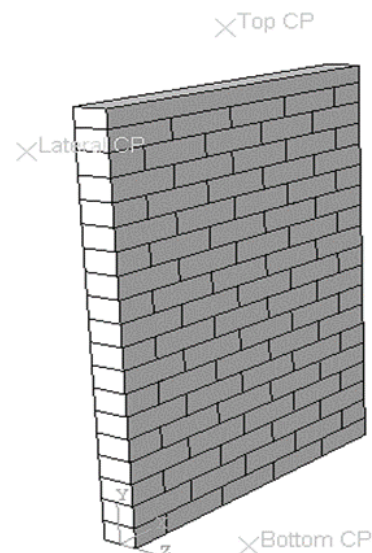Using the SMM technique explained in section 2, a numerical model of an unreinforced masonry wall of dimen-

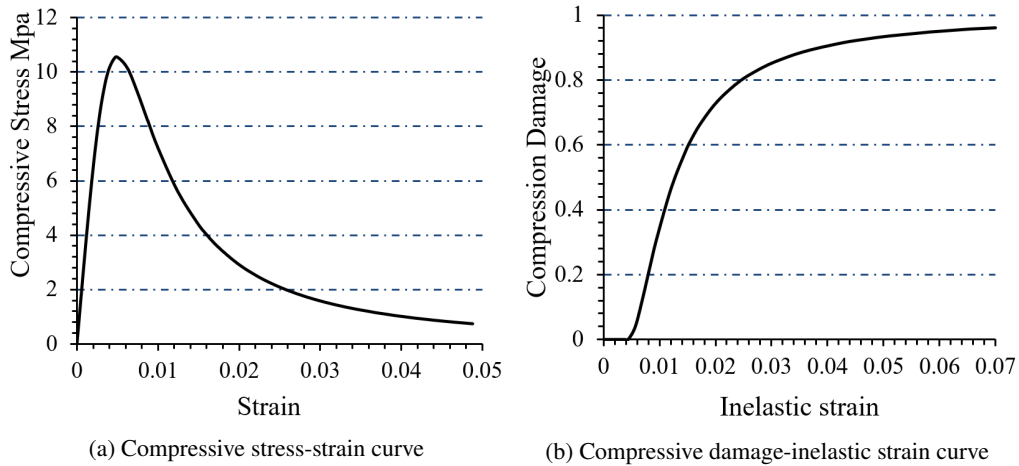Figure 2: Numerical model of an unreinforced masonry wall in ABAQUS

(a) Compressive stress-strain curve   (b) Compressive damage-inelastic strain curve

Figure 3: Constitutive model for masonry units in compression

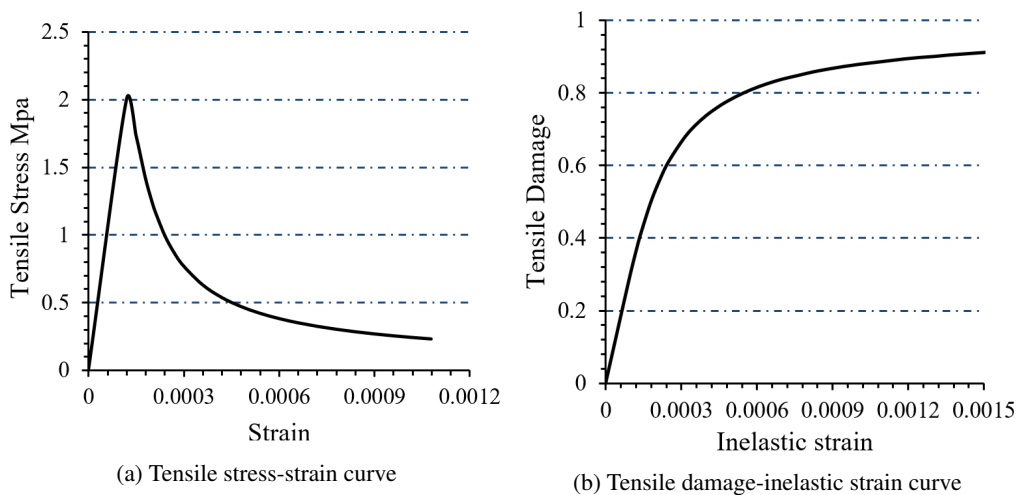(a) Tensile stress-strain curve   (b) Tensile damage-inelastic strain curve

Figure 4: Constitutive model for masonry units in tension

sion (990 x 1106x 100) mm is prepared in ABAQUS. Depending upon position of brick units, six different sizes of masonry units (four different full brick size: 220 x 57 x 100, 220 x 62 x 100, 215 x 57 x 100, and 215 x 62 x 100, and two different half brick size: (115 x 57 x 100 and 115 x 62 x 100) mm, obtained by expanding brick units in single or both directions along vertical and horizontal direction to include thickness of mortar, are used to simulate the numerical model. The masonry units expanded vertically in only one direction are used in the top and bottom layers in the numerical model. Three different reference points namely Bottom CP, Top CP, and Lateral CP are created for coupling purposes through which the boundary conditions and loads are assigned during the simulation process. A single steel beam of dimension (990 x 50 x 100) mm is provided at the top of the wall to apply vertical load through the top CP and horizontal displacement is provided in the top layer of a brick through the lateral CP point of the subject model as shown in Figure 2.

The elastic properties and non-linear material properties of constitutive materials and joint interface used for the simulation of the numerical model of masonry wall are based on the previous research work conducted by Lourenço, 1996 and Kurdo et al., 2017. The mechanical properties of masonry units and steel beam is shown in Table 2.

Based on the theory of CDP model, the stress-strain and damage-inelastic strain relationship for masonry in compression and tension are shown in Figure 3 and Figure 4

Table 2: Material properties of masonry units and steel beam

S.No.	Component	Parameters	Value	Source
1	Masonry Units	Density (ρ), Kg/m^3	2000	Kurdo et al., 2017
2		Elastic modulus (E), Mpa	167000	Kurdo et al., 2017
3		Poisson's ratio (ν)	0.15	Kurdo et al., 2017
4		Compressive strength (F_c), Mpa	10.5	Kurdo et al., 2017
5	Steel Beam	Tensile strength (F_t), Mpa	2.0	Kurdo et al., 2017
6		Density (ρ_s), Kg/m^3	7800	Kurdo et al., 2017
7		Elastic modulus (E_s), Mpa	200000	Kurdo et al., 2017
8		Poisson's ratio (ν_s)	0.25	Kurdo et al., 2017

Table 3: Properties of joint interface

S. No.	Parameters	Value	Source
1	Cohesion (c), Mpa	0.35	Kurdo et al., 2017
2	Frictional coefficient (μ)	0.75	Kurdo et al., 2017
3	Tensile strength ($\sigma_n^{\max}$), Mpa	0.25	Kurdo et al., 2017
4	Shear strength ($\sigma_s^{\max}$)	0.25	Kurdo et al., 2017
5	Normal tensile stiffness (K_{nn})	81.8	Equation 4
6	Shear stiffness (K_{ss})	36.4	Equation 5
7	Tensile fracture energy (G_{nf})	1.91	Equation 10
8	Shear fracture energy (G_{sf})	19.1	Equation 11

respectively. The stress-strain relationship for compression is linear up to the ultimate strain of 0.003. Beyond this, the response in the plastic zone is characterized by stress hardening up to peak stress σ_c corresponding to peak strain 0.005, followed by stress-strain softening beyond this peak stress. For uniaxial tension, the stress-strain relationship is linear up to peak stress σ_t, followed by stress-strain softening. The stress-strain softening refers to the propagation of micro-cracks.
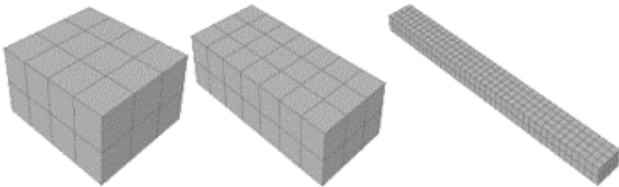

Figure 5: Generated mesh of individual constituents

The properties of the joint interface used between masonry units for numerical simulation are summarized in Table 3. For simulation, the base of the numerical model is initially restrained through the bottom CP about all axes followed by the application of a vertical load of 29.7 KN (corresponding to 0.3 MPa) through the top CP. After the application of vertical load, the vertical and out-of-plane horizontal movement of the top beam is restrained and an incremental in-plane horizontal displacement of 4 mm is applied on the model through the top layer of brick allowing the masonry

assemblage to move only in the direction of force applied. The vertical load is applied constantly throughout the simulation period. A linear 8-noded explicit material C3D8R is adopted with reduced integration and enhanced glass hour control for each masonry unit with a seed size of 30 mm for meshing purposes. Similarly, a seed size of 25 mm with the same element topology is adopted for the steel beam as shown in Figure 5. The mesh size was chosen based on a mesh sensitivity study performed by Kurdo et al., 2017.

3.3. Verification of model

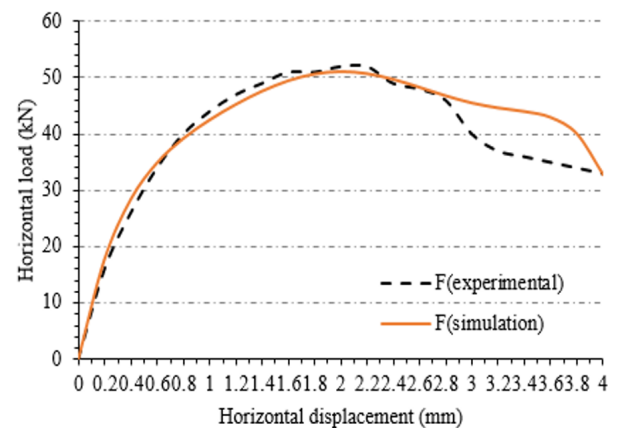#### 3.3.1 Comparison of pushover curve

Figure 6: Comparison of pushover curve for validation

For validation of the numerical model, the pushover curve obtained from numerical simulation is compared with experimental results given by Kurdo et al., 2017. Figure 6 shows a good arrangement with experimental results up to the ultimate load capacity. The coefficient of regression (R square) is found to be 93.30% with a standard deviation of 12.625. The peak strength of masonry assemblage is found to be 51.14 kN which is 1.7% less than that of the experimental result corresponding to 52 kN. The nature of the degradation of lateral stiffness of the numerical model after the peak point is slightly different from experimental results.

3.3.2 Comparison of damage pattern

(a)   (b)
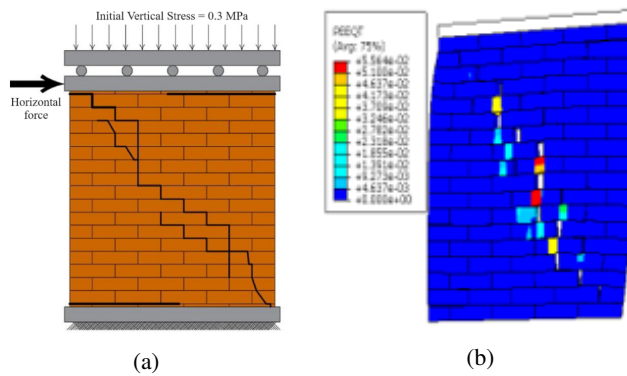
Figure 7: Comparison of damage pattern of an unreinforced masonry wall: (a) experimental failure patterns (b) Failure pattern in numerical model represented by PEEQT at total step time of 0.25 sec (scale factor = 20)

The cracking of masonry units is represented by the distribution of tensile equivalent plastic strain (PEEQT) in ABAQUS and the cracking in masonry units initiates at a point where PEEQT is greater than zero. Under the action of lateral load, the tensile cracks are developed at the top and bottom of the wall initially followed by continuously increasing tensile cracks at the top and bottom of the wall without evolution of PEEQT until the critical cracking point is reached. The value of PEEQT increases with an increase in lateral loading representing increasing in the cracking of masonry units. A diagonal steeped crack between masonry units is observed followed by the crushing of masonry units under compression at the top and bottom toes as represented in Figure 7 which resembles experimental results as defined by Kurdo et al., 2017. The crushing of masonry units is represented by the distribution of compressive damage variable (DAMAGEC). The masonry units are crushed when the uniaxial strain corresponding to DAMAGEC reaches the crushing strain of masonry units. Figure 8 represents the distribution of DAMAGEC on the masonry wall along with di-

agonal steeped cracking and tensile cracking at the top and bottom of the wall.
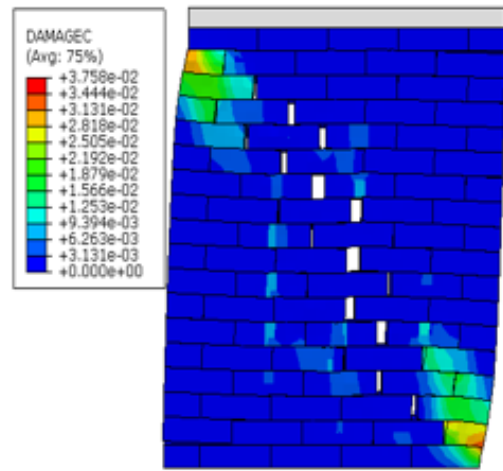

Figure 8: Evolution of cracks pattern represented by DAMAGEC at 4mm horizontal displacement at top (scale factor = 20)

3.3.3 Comparison of stress transfer mechanism

The evolution of the stress transfer pattern in the masonry wall is represented by minimum principal compressive stress (S, Min. Principal). For the initial stage of loading, the lateral load is transferred through the diagonal of the masonry wall resulting in the formation of a diagonal strut as represented in Figure 9. The formation of a diagonal strut resembles the actual behavior of the typical unreinforced masonry wall.
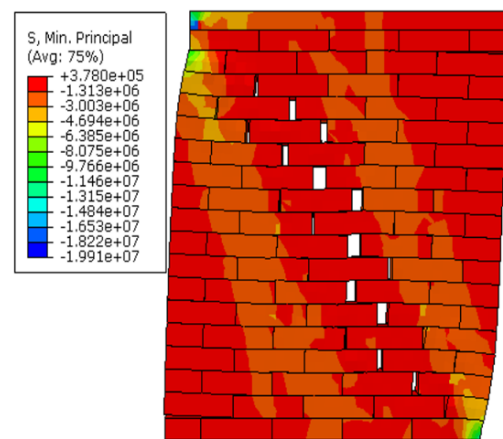

Figure 9: Formation of diagonal strut represented by distribution of minimum principal stress distribution with crack patterns at 4 mm horizontal displacement at top (scale factor = 20)

Table 4: Material properties for steel strips and anchor bolts

Parameters	Steel strip	Anchor bolts (Grade 8.8)
Density (ρ_s), Kg/m^3	7800	7800
Poisson's ratio (ν_s)	0.3	0.3
Elastic modulus (E_s), MPa	200000	200000
Yield strength (σ_{ys}), MPa	250	648
Tensile strength (σ_{ts}), MPa	797	797
Elastic modulus in hardening zone (E_h), MPa	2000	2000
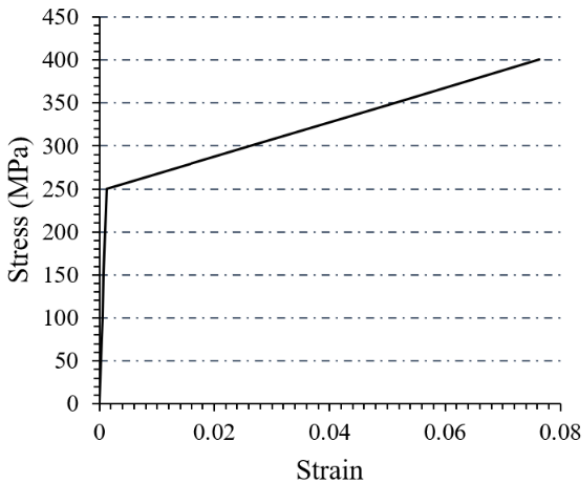
(a) Stress-strain distribution for steel strip
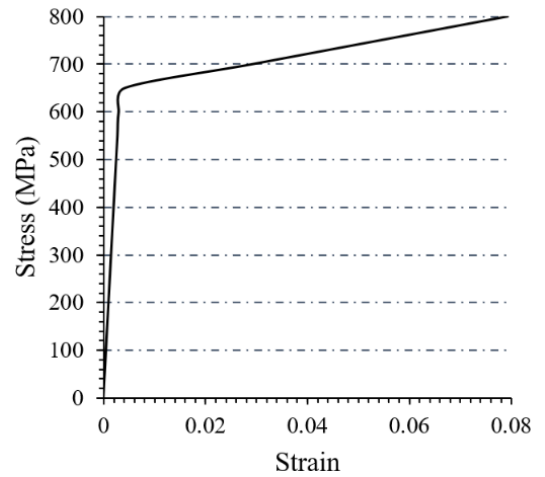
(b) Stress-strain distribution for anchor bolt

Figure 10: Stress-Strain relationship for steel strip and anchor bolts

4. Finite element analysis of reinforced masonry wall panel

After the validation of the numerical model, the same wall panel without any changes in geometry, mechanical properties, boundary, and loading conditions is reinforced. The finite element model of the reinforced masonry wall panel is prepared to study the changes in the behavior of the wall. A stainless strip of dimension (1200 x 50 x 3) mm is provided diagonally on both sides of the masonry wall where tensile stress is developed under lateral loading, mechanically attached by 3 nut-bolt arrangement of nominal diameter 12 mm at 400 mm c/c through drilling holes on masonry units. The separation of bolts is based on the basic assumption of buckling behavior when provided at higher spacing other than (300 to 400) mm (Borri et al., 2019).

The mechanical properties of masonry units and steel beams are similar to those in unreinforced masonry walls. The classical plasticity model with isotropic hardening behavior is used for steel strips and bolts. Table 4 summarizes the mechanical properties of steel strips and anchor bolts representing linear and non-linear behavior. The stress-strain distribution for steel strips and anchor bolts is shown
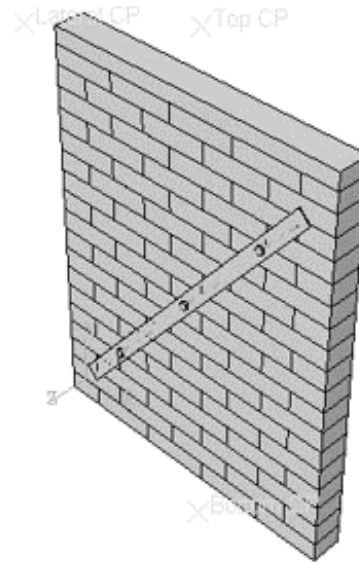

Figure 11: Numerical model of a reinforced masonry wall panel in ABAQUS

in Figure 10. The interface model used to define the response of joint material between masonry units in unreinforced masonry walls is again used here to redefine the linear and non-linear response of joint interface in reinforced masonry wall panels. The tie-type coupling is used between the lateral circumferential surface of the anchor rod and each core of the borehole drilled in masonry units to represent the embedded nature of the anchor bolt in the masonry wall. The tangential and normal behavior are only used to define the interaction between steel surfaces. No consideration is made for interaction between the steel surface and masonry surface in a lateral direction. It is assumed that the steel strips carry stresses or loads through anchor bolts only, not from the lateral surface of the masonry wall. The normal behavior is assigned as 'hard contact' using default constraint enforcement with separation allowed after contact. Tangential behavior is assigned using penalty friction formulation with a friction coefficient of 0.1. Figure 11 represents a numerical model of reinforced masonry wall panels with a simple arrangement of steel strips and anchor bolts.

The loading and boundary conditions are kept similar to unreinforced masonry wall panels. The vertical compression load of 0.3 MPa is applied to the reinforced masonry panel through the upper coupled reference point in the first step. In the second step, after the completion of vertical loading, the in-plane monotonic load in terms of lateral displacement is applied through the top layer of the wall panel maintaining constant vertical compression stress provided that the vertical and out-of-plane horizontal displacement as well as rotation about all axes are restrained.

Every masonry unit is independently meshed with a seed size of 25 mm to maintain a uniform distribution of meshing so that the meshing of masonry units with drilled holes does not cause problems in transferring stress and force. A special sweep technique with medial axis mesh transition is used around the region of circular holes for effective transfer of force and stress as concentration is high in these regions of holes. A similar provision is provided for the meshing of steel strips and the bolts used for reinforcing purposes as shown in Figure 12.
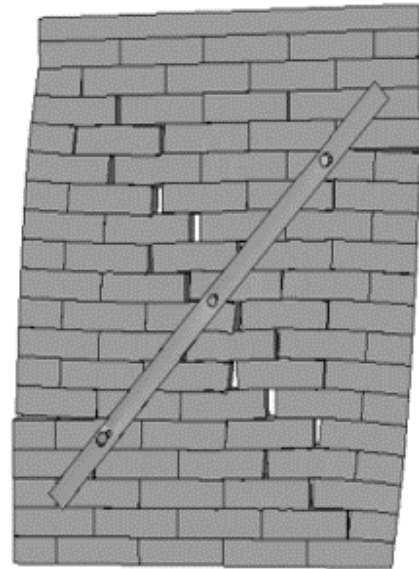
Figure 13: Damage pattern of reinforced masonry wall panel with all units intact (Scale factor = 20)

The numerical model of the reinforced masonry wall panel is simulated under vertical stress of 0.3 MPa and displacement-controlled horizontal loading of 4 mm. Figure 13 represents the damaged pattern of the reinforced masonry wall panel. The response of the reinforced masonry wall is represented by Figure 14. The ultimate load-carrying capacity is found to be 62.324 kN corresponding to 2.6 mm displacement.
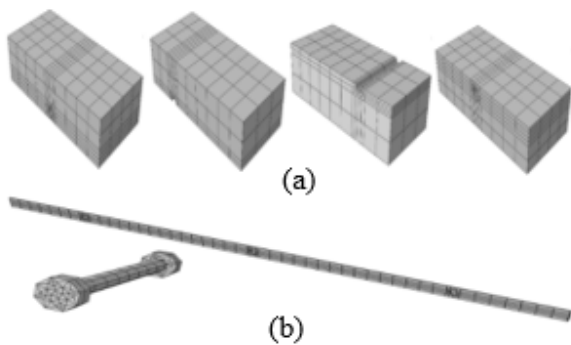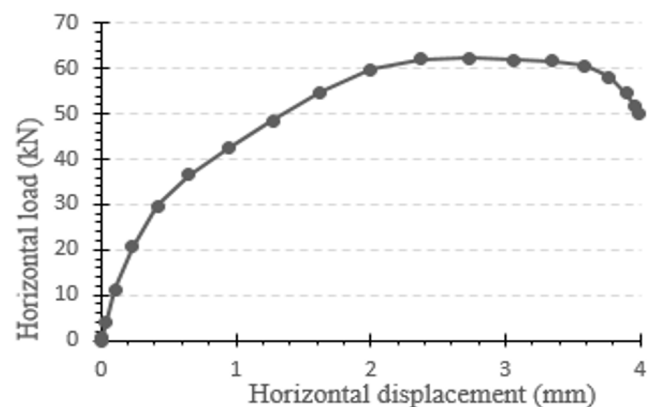

Figure 12: Different meshed units used in numerical modeling of reinforced masonry wall panel: (a) meshed masonry units with boreholes (b) meshed steel strip and anchor bolt

Figure 14: Force-displacement curve for reinforced masonry wall panel

5. Result and Discussion

Figure 15 represents the change in shear strength of reinforced and unreinforced masonry wall panels. The peak strength of a masonry wall reinforced with steel strips on both sides of the wall is about 22% higher compared to that of an unreinforced masonry wall. The secant stiffness of the reinforced masonry wall panel at peak strength decreased by about 7% and the ductility factor at ultimate load decreased by about 21% compared to that of the unreinforced masonry wall panel. This reduction of secant stiffness and ductility factor is due to the higher yield displacement of reinforced masonry wall panels due to the use of steel strips as reinforcing materials. The distribution of the maximum value of PEEQT at the peak point decreased by about 70% resulting in less cracking of masonry units and less diagonal steeped cracks. Similarly, the maximum value of DAMAGEC at ultimate load decreased by 4% which represents significant prevention of toe crushing or compressive crushing of masonry units in the reinforced masonry wall panel compared to that of the unreinforced masonry wall panel.
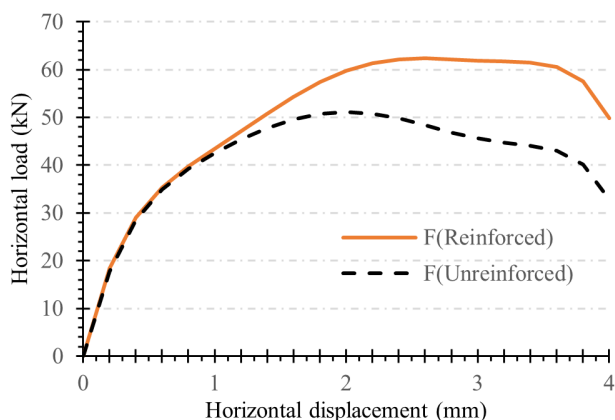

Figure 15: Comparison of non-linear behavior of unreinforced and reinforced masonry wall panel

6. Conclusion and Recommendations

In this research work, the real behavior of the URM wall panel under monotonic lateral loading is accurately simulated using the numerical simulation method. The adequacy of the finite element technique was accessed by validating the response of the URM wall panel against experimental results particularly based on the failure mechanism, damage pattern, and stress transfer mechanism. The study shows that the lateral load-carrying capacity of reinforced masonry wall panels under displacement-controlled monotonic lateral loading increased by about 22% using steel strips and anchor bolt arrangement as a reinforcing method. Future research work can include the study of the effect of different aspect ratios for analysis of load carrying capacity of masonry wall panels. In this study, an aspect ratio of unity is used for which the diagonal mode of failure is predominant. Similarly, the behavior of walls under different values of pre-compression stress can be studied in the future. Only in-plane monotonic loading is considered in this study. The behavior of masonry walls under cycling loading and the out-of-plane behavior of masonry can be considered in future studies.

References

Aref, A. J., & Dolatshahi, K. M. (2013). A three-dimensional cyclic meso-scale numerical procedure for simulation of unreinforced masonry structures. *Computers and Structures*, *120*, 9–23. https://doi.org/10.1016/j.compstruc.2013.01.012

Benzeggagh, M. L., & Kenane, M. (1996). Measurement of mixed-mode delamination fracture toughness of unidirectional glass/epoxy composites with mixed-mode bending apparatus. *Composites Science and Technology*, *56*, 439–449.

Borri, A., Corradi, M., Castori, G., & Molinari, A. (2019). Stainless steel strip – a proposed shear reinforcement for masonry wall panels. *Construction and Building Materials*, *211*, 594–604. https://doi.org/10.1016/j.conbuildmat.2019.03.197

Kurdo, F., Lee, S., Simulating, M., Abdulla, K. F., Cunningham, L. S., & Gillie, M. (2017). Simulating masonry wall behaviour using a simplified micro-model approach. *Engineering Structures*, *151*, 349–365. https://doi.org/10.1016/j.engstruct.2017.08.021

Lee, J., & Fenves, G. L. (1998). Plastic-damage model for cyclic loading of concrete structures. *Journal of Engineering Mechanics*, *124*(8), 892–900. https://doi.org/10.1061/(asce)0733-9399(1998)124:8(892)

Lotfi, H. R., & Shing, P. B. (1994). Interface model applied to fracture of masonry structures. *Journal of Structural Engineering*, *120*(1), 63–80.

Lourenço, P. B. (1996). *Computational strategies for masonry structures*.

Lubliner, J., Oliver, J., Oller, S., & Onate, E. (1989). A plastic-damage model for concrete. *International Journal of Solids and Structures*, *25*(3). https://doi.org/10.1016/0020-7683(89)90050-4

Qingfu, L., Wei, G., & Yihang, K. (2020). Parameter calculation and verification of concrete plastic damage model of ABAQUS. *IOP Conference Series: Materials Science and Engineering*, *794*(1). https://doi.org/10.1088/1757-899X/794/1/012036

Raijmakers, T. M. J., & Vermeltfoort, A. T. (1992). *Deformation controlled tests in masonry shear walls: Report B-92-1156*.

Wang, C., Sarhosis, V., & Nikitas, N. (2018). Strengthening/retrofitting techniques on unreinforced masonry structure/element subjected to seismic loads: A literature review. *The Open Construction and Building Technology Journal*, *12*(1), 251–268. https://doi.org/10.2174/1874836801812010251

Yuen, T. Y. P., Deb, T., Zhang, H., & Liu, Y. (2019). A fracture energy based damage-plasticity interfacial constitutive law for discrete finite element modelling of masonry structures. *Computers and Structures*, *220*, 92–113. https://doi.org/10.1016/j.compstruc.2019.05.007

Zhang, S., Yang, D., Sheng, Y., Garrity, S. W., & Xu, L. (2017). Numerical modelling of FRP-reinforced masonry walls under in-plane seismic loading. *Construction and Building Materials*, *134*, 649–663. https://doi.org/10.1016/j.conbuildmat.2016.12.091